

Elucidating CO₂ nanobubble interfacial reactivity and impacts on water chemistry

Gabriel Antonio Cerrón-Calle^a, Andre Luna Magdaleno^a, John C. Graf^b, Onur G. Apul^c,
Sergi Garcia-Segura^{a,*}

^a Nanosystems Engineering Research Center for Nanotechnology-Enabled Water Treatment, School of Sustainable Engineering and the Built Environment, Arizona State University, Tempe, AZ 85287-3005, USA

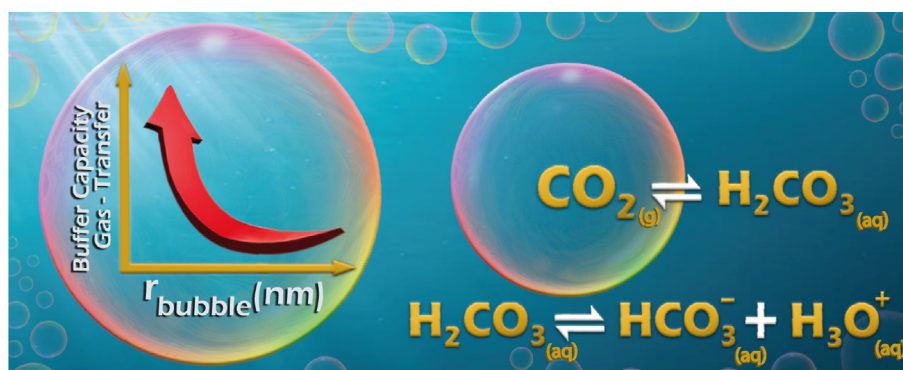
^b NASA Johnson Space Center, Houston 77058, TX, United States

^c Department of Civil and Environmental Engineering, University of Maine, Orono 04469, ME, United States

HIGHLIGHTS

- CO₂ nanobubbles increase mass transfer coefficient (K_{La}) respect traditional bubbles.
- Nanobubble size distribution determined by nanotrack analysis.
- CO₂ nanobubble size distribution is affected by pH change.
- Nanobubbles solutions have 7 times higher buffering capacity.

GRAPHICAL ABSTRACT



ARTICLE INFO

Article history:

Received 10 August 2021

Revised 4 September 2021

Accepted 6 September 2021

Available online 8 September 2021

Keywords:

Buffer capacity

Gas transfer

Nanoparticle track analysis

Nanointerfaces

ABSTRACT

Hypothesis: Carbon dioxide nanobubbles can increase effective gas-transfer to solution and enhance buffering capacity given the stable suspension in water of CO₂ gas within nanobubbles and the existence of larger gas/water interface.

Experiments: The physico-chemical properties and responses of CO₂ nanobubbles were recorded at different generation times (10, 30, 50, and 70 min) and benchmarked against traditional macrobubbles of CO₂ for the same amount of delivered gas. Effective concentration of CO₂ was evaluated by measuring the buffer capacity (β). The size distribution of nanobubbles during the experiments was measured by Nanoparticle Track Analysis.

Findings: The mass transfer coefficient (K_{La}) showed a dramatically increase by 11-fold for the same volume of gas delivered when using nanobubbles. The β values obtained for nanobubbles were 7 times higher than that of traditional bubbles which can lead to significant source of CO₂ availability by using the nanobubble method. Nanobubbles, consequently, undergo mass loss at higher pH corresponding to mass transfer process due to concentration gradient at the surrounding nanobubbles. This is the first report of CO₂ nanobubbles buffer capacity evaluation.

© 2021 Elsevier Inc. All rights reserved.

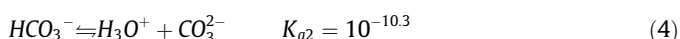
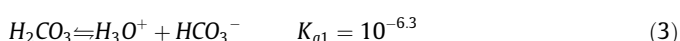
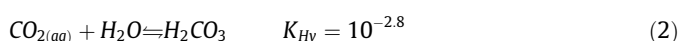
* Corresponding author.

E-mail address: Sergio.garcia.segura@asu.edu (S. Garcia-Segura).

1. Introduction

Nanobubbles (NBs) are stable tiny gas-filled cavities in liquid phase with a dimension range of 50 to 1000 nm [1,2]. NBs are defined into two conditions: attached to surfaces (surface nanobubbles) or suspended in spherical shape in the solution (bulk nanobubbles) [3,4]. NBs are thermodynamically metastable nanointerfaces that can remain in solution for days, weeks, and even months [5–7]. In traditional macro bubbles, the buoyancy force induces bubbles to ascend. However, buoyancy forces are insignificant for NBs contributing to their outstandingly extended suspension in solutions [4]. The high residence time of bubbles in water has been explained by the negligible buoyancy and their transport only through Brownian motion [8,9]. The interest in nanobubbles come from their unique properties such as stability [10], large interfacial surface area [11], and reactive oxygen species [12]. Oxygen, nitrogen, and air NBs are the most common type of gases studied as NBs. Oxygen NBs present interesting properties in plants growth [13,14], generation of reactive oxygen species (ROS) [8,12], and mass transport studies [15,16]. Nitrogen and air NBs were studied in well-known systems to evaluate the influence of NBs in different applications such as food production [17] and water treatment [18,19].

Carbon dioxide (CO₂) NBs have a substantial difference with the previously studied gas systems since CO₂ is an acid gas that reacts with water. The dissolution of CO₂ in water generates the natural bicarbonate system in aquatic chemistry [15,20]. This system involves three physico-chemical processes: i) gas–liquid transfer described by reaction (1) that is dominated by Henry's Law, ii) the reaction of CO₂ with water yielding carbonic acid according to reaction (2), and the acid-base equilibrium of carbonic acid as weak acid following reactions (3)–(4) [21,22].



Therefore, the CO₂ in water forms an acid buffer in which capacity depends on the amount of CO₂ dissolved in water. Acid buffer solutions have a wide frame of applications in various fields and it is of high environmental relevance [23,24]. The limiting steps of CO₂ absorption in water is ascribed to CO₂ solubility and the gas–liquid phase equilibrium. Chemical reactions and gas transfer processes in respect to the same NB system have been seldomly explored. In the case of CO₂, NBs could behave as an additional source of CO₂ for a chemical reaction (bicarbonate system), modify solution pH, or even provide additional carbon source to a carbon-starving system (e.g., algae growth) [20]. NBs hold the promise of overcoming the solubility barrier by providing a pragmatic source of CO₂ retained in solution. This differential element makes CO₂ nanobubbles extremely interesting and provide a unique opportunity to further understand gas–liquid nanointerfaces to outline future application of NBs. These are few applications that can be a game-changing for space exploration, life-support systems, CO₂ capture, and resource recovery by providing relevant uses to CO₂ resulting from astronauts' respiration and fuel combustion [25].

Few reports in literature present studies on the formation and stability of CO₂ nanobubbles, and those are mostly related to food applications [6,26] and bactericidal activity [27]. Also, fundamental studies have been reported the longevity [6], radical activity [28], interaction with ions [29], and zeta potential values [30] of CO₂ nanobubbles. However, buffer capacity of the system and gas-

transfer coefficient are still unknown for these new systems. This work advances the fundamental understanding on the positive effects of gas/water nanointerfaces enabled by the long-term residence of CO₂ nanobubbles in solution, which may open new avenues to exploit in different science and engineering areas that are experiencing low process efficiencies due to the limitation of CO₂ mass transfer and/or inefficient gas delivery to aqueous phase.

In this study, CO₂ NBs generation was experimentally investigated regarding stability, formation, acid-base characteristics, and buffer capacity. In addition, the different behavior of NBs was benchmarked against conventional CO₂ macro-bubbles. The physical stability and properties of NBs was monitored at different values of pH providing insights on the fundamental mechanisms of reacting NBs. Probably, this is the first study that reports the gas-transfer coefficient and buffer capacity for CO₂ nanobubbles.

2. Materials and methods

2.1. Generation of nanobubbles and conventional bubbling procedures

Carbon dioxide nanobubbles were generated using the batch recirculation system (see Fig. 1) using a Moleaer nanobubble membrane generator model XTB 25 GPM. The experiment was performed in a 210 L high density polyethylene barrel that was coupled to a nanobubble generator. All experiments were conducted with 50 L of deionized water. The system used had a reflux connection to concentrate nanobubbles in solution. All tubes and gas lines of experiment were connected by Swagelok nuts and ferrules to avoid leaking. Pressurized pure CO₂ gas (>98%) purchased from Arizona State University gases was used as CO₂ source. The CO₂ was delivered to the NB generator under 2.7×10^5 Pa and constant flowrate of 0.7 L min⁻¹. Generation of NBs was maintained for 70 min and samples were collected at different times of 10, 30, 50 and 70 min. The pH and conductivity were registered during the generation of NBs and after the sample collection using a Thermo Scientific Orion Star A221 meters.

Meanwhile, conventional macrobubbles were generated using a by-pass configuration from the nanobubbles system to control the gas inlet and keeping gas flowrate of 0.7 L min⁻¹ (1.5 SCFH) as a constant parameter for comparison. Samples were collected at 10, 30, 50 and 70 min. Similarly, pH and conductivity were monitored during the bubbling process.

2.2. Nanobubbles and nanobubble solutions characterization

The size distribution of the NBs was determined using a Nanoparticle Tracking Analysis (NTA) Nanosight NS300 (Malvern). The particles diameter was then calculated using the Stokes-Einstein equation (5):

$$\frac{\Delta R^2(t)}{4t} = D = \frac{k_B T}{6\pi\eta r} \quad (5)$$

where k_B is the Boltzmann's constant (1.380649×10^{-23} J K⁻¹), T is the temperature in K, and η is the liquid viscosity in N s m⁻², and r is the nanoparticle radius in nm. Based on Brownian motion of the particle, the diffusion coefficient (D) was estimated using the relationship $\Delta R^2(t) = |r_1(t) - r_1(0)|^2$ that is the mean square displacement of the particle measured by the NTA at a given time t . Samples were recorded three times during 60 s periods with a low threshold noise value of 6 and a camera level 14 maintaining a good relationship of bright and contrast. Before each measurement, sample was advanced to focus on different nanobubbles.

The zeta potential of the NBS was measured with a NanoSight 90 PALS (Brookhaven) instrument. Measurements were conducted under multiple cycle mode (15 cycles per measurement) and each

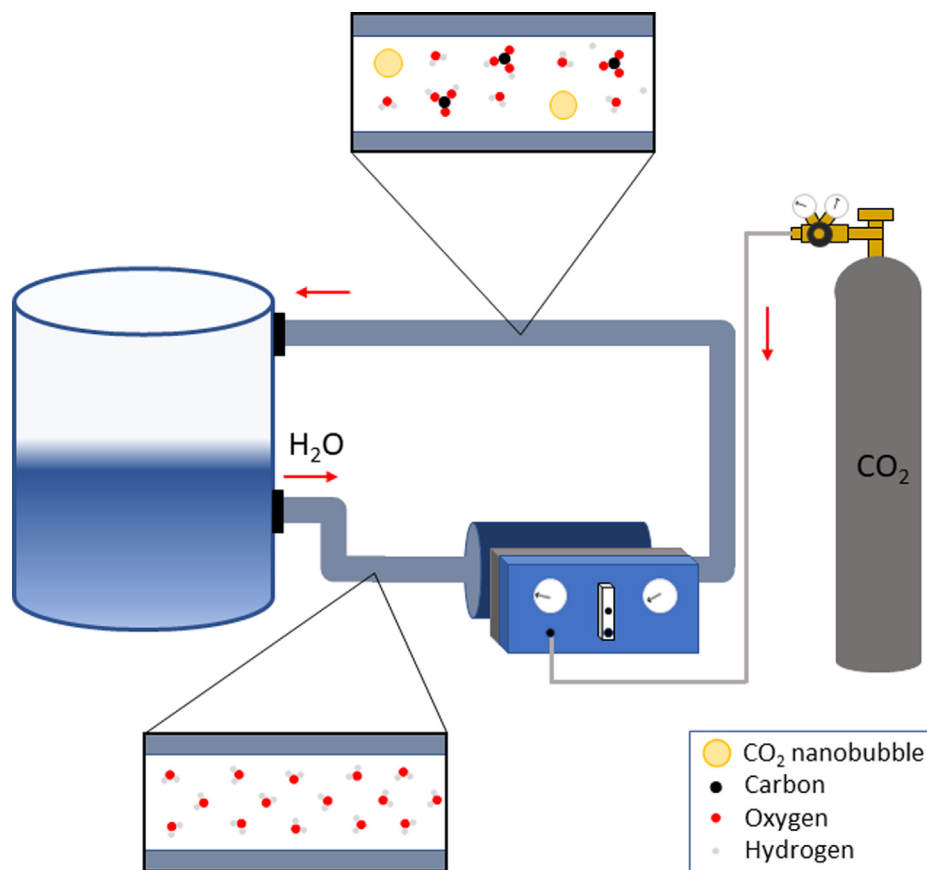


Fig. 1. Scheme of experimental set up for CO₂ bulk nanobubbles generation.

sample analyzed in quintuplicate. The zeta potential was calculated according to the Smoluchowski model.

The buffering capabilities of the NBs solution and the macrobubble CO₂ solution were evaluated by titration using 0.1 mol L⁻¹ NaOH. Solutions of NaOH were prepared with analytical grade NaOH pellets provided by Sigma-Aldrich. The true concentration of NaOH titrant was determined using primary standard potassium hydrogen phthalate (>99%, Sigma-Aldrich). The buffer capacity (β) was quantified following equation (6):

$$\beta = \frac{n}{\Delta pH} \quad (6)$$

where n is the number of moles of acid/base added per liter of buffer over the change of pH (ΔpH).

3. Results and discussion

3.1. Understanding water chemistry changes induced by CO₂ bulk nanobubbles

Dissolution of CO₂ in water yields carbonic acid according to reaction (2). Thus, CO₂ is considered an acid gas that can modify pH of water. The change of water acidity has been positively exploited in carbonated drinks. However, the carbonate system chemistry has arisen concerns given the drastic change of oceans pH by uncontrolled CO₂ gas emissions [24]. To better understand the role of NBs on water chemistry, pH and conductivity was monitored during their generation in the 50 L of treated solution. Fig. 2 illustrates these physico-chemical changes over time for both conventional macrobubbling of CO₂ and NBs generation. The initial solution pH of 5.8 gradually decreases over time generating a buf-

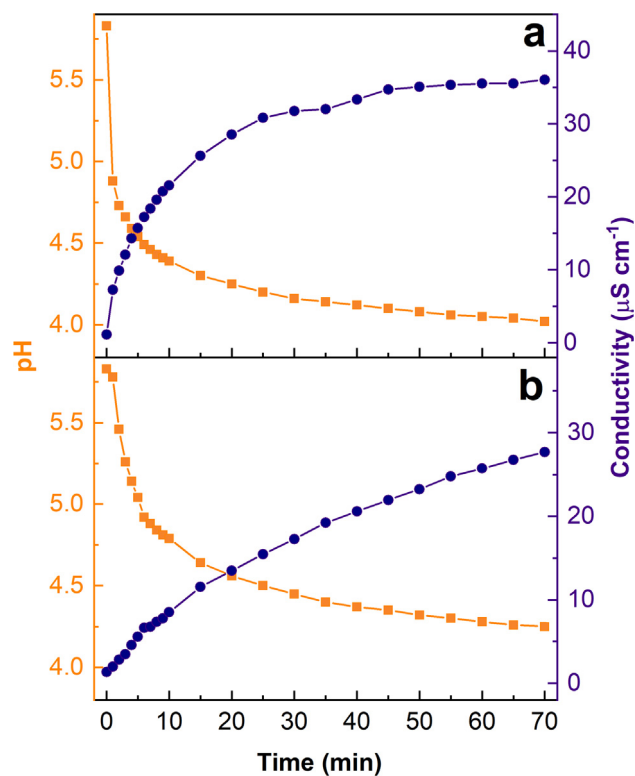


Fig. 2. Time-course change of (■) pH and (●) conductivity during (a) generation of nanobubbles of CO₂ and (b) direct bubbling of CO₂ macrobubbles. The experiments conducted in triplicate showed a deviation standard < 2%.

fer solution in both cases \sim pH 4. However, there is a drastic increment on the pH change rate observed for NBs when compared to macrobubbles. Conventional bubbling attains a value of pH 4.5 in 25 min whereas through NBs generation pH 4.5 is attained in 5 min, a 5-fold faster pH change induced by CO₂ NBs. The change of pH is directly related to the solubilization kinetics, thus is directly related to the gas transfer process to the aqueous phase. According to the two-film model it can be assumed the presence of a hypothetical stagnant film layer on both sides of a gas–liquid interface defined by the gas bubble in solution [3]. Then, the transfer of CO₂ gas to the liquid phase occurs following three sequential stages: (i) molecular diffusion across the gas film of thickness δ_G , interfacial equilibrium, and molecular diffusion across the gas film of thickness δ_L . Assuming that the air–water interface is extremely thin and that the flux on the gas side equals the flux on the liquid side in magnitude, the mass transfer coefficient in each phase should contribute to the overall resistance to the transport. In this frame, the overall mass transfer coefficient (K_L) can be expressed as the additive mass transfer resistances according to equation (7):

$$\frac{1}{K_L} = \frac{1}{k_L} + \frac{1}{K_H k_G} \quad (7)$$

where k_L is the mass-transfer coefficient at the liquid-side, k_G is the mass-transfer coefficient at the gas-side, and K_H is the dimensionless Henry's constant for CO₂ in water ($10^{-1.5}$ at 25 °C). In engineering systems, the mass transfer depends on the reactor vessel and are usually normalized by defining engineering constant $K_L a$ as a volumetric mass transfer coefficient that takes into account not only film and compound properties, but also the specific surface area for mass transfer in a given reactor. According to Kordač at pH < 5 the concentration of H₂CO₃ can be described using the following expression (8):

$$\frac{dC_{H_2CO_3}}{dt} = K_L a \left(\frac{A}{1+A} \right) (C_{H_2CO_3^*} - C_{H_2CO_3}) 0.99 \quad (8)$$

Where $K_L a$ is the volumetric mass transfer coefficient in h⁻¹, $C_{H_2CO_3^*}$ is the concentration of physically dissolved CO₂ and H₂CO₃ in equilibrium with p_{CO_2} in the gas phase defined by Henry's law expressed in mol L⁻¹. The concentration $C_{H_2CO_3^*}$ at equilibrium conditions is defined by Henry's law (9):

$$C_{H_2CO_3^*} = \frac{P_{CO_2}}{H} = P_{CO_2} * 10^{-(5.3 - \frac{1140}{T})} \quad (9)$$

$C_{H_2CO_3}$ is the experimentally measured concentration in solution expressed in mol L⁻¹, and A is a complex term defined as follows in equation (10):

$$A = \frac{QH}{K_L a V R T} \quad (10)$$

Where Q is the aeration rate in L s⁻¹, H is the Henry's coefficient of CO₂ that is 31.62 atm L mol⁻¹ at 25 °C, V is the volume of the system in L, R is the ideal gas constant 0.082 atm L⁻¹ K⁻¹ mol⁻¹, and T is the temperature in K.

Equation (8) can be further simplified as shown in equation (11) by defining the term B that compiles all the constant terms of the system (see eq. (12)).

$$B = K_L a \frac{A}{1+A} 0.99 \quad (11)$$

$$\frac{dC_{H_2CO_3}}{dt} = B (C_{H_2CO_3^*} - C_{H_2CO_3}) \quad (12)$$

The definite integration of the former differential equation between the concentration $C_{H_2CO_3}$ at time 0 and the concentration at time t yields equation (13) that is linearized with natural logarithm as defined by equation (14),

$$C_{H_2CO_3(t)} = C_{H_2CO_3^*} - [C_{H_2CO_3^*} - C_{H_2CO_3(0)}] e^{-Bt} \quad (13)$$

$$B = - \frac{\ln \left(\frac{C_{H_2CO_3^*} - C_{H_2CO_3(t)}}{C_{H_2CO_3^*} - C_{H_2CO_3(0)}} \right)}{t} \quad (14)$$

Meanwhile the concentration at time t can be calculated from the experimental pH followed during CO₂ bubbling as defined by equation (15):

$$C_{H_2CO_3(t)} = \frac{10^{-2pH(t)}}{K_{a1}} \quad (15)$$

where K_{a1} is the equilibrium constant of the acid-base reaction of H₂CO₃ of 8.15×10^{-7} M⁻¹. Finally, we can determine the $K_L a$ from equation (16):

$$K_L a = \left[\frac{0.99}{B} - \frac{VRT}{QH} \right]^{-1} \quad (16)$$

The $K_L a$ value determined for CO₂ NBs is 0.35 h⁻¹, which is 11-fold higher than the registered for conventional bubbling of 0.03 h⁻¹. This marked difference can be explained by the larger interfacial area of CO₂ NBs and their continuous suspension in solution, which increases the contact time. In contrast, large macrobubbles of CO₂ have a larger volume of gas that never gets in contact with the liquid interface and leave the reactor due to gas buoyancy. The hydraulic retention time of a macrobubble ($r_b < 0.01$ -cm) in the reactor can be estimated from the bubble rise velocity (U_b) assuming Stokes law regime by equation (17) [31]:

$$U_b = \frac{1}{3} \left(\frac{g r_b^2}{\gamma} \right) \quad (17)$$

where g is the gravity constant of 9.80665 m s⁻², r_b is the bubble radius, and γ is the kinematic viscosity of water of 0.801 mm² s⁻¹ at 25 °C. Thus, small macrobubbles of 0.01 cm will have a U_b of 0.04 m/s with an estimated retention time in the reactor of 13.47 s considering vertical buoyancy rising in the solution height of 55 cm. The different scale of contact time between macrobubbles and NBs provides a holistic view on the higher efficacy of gas usage when considering NBs.

In the case of conductivity, the initial conductivity was around 1.578 μS cm⁻¹ and final conductivity values for CO₂ nanobubbles was 36.05 μS cm⁻¹, meanwhile for CO₂ macrobubbles it was 27.67 μS cm⁻¹. The increase on conductivity is explained by the yield of ionic species (i.e., HCO₃⁻) following reactions (2) and (3). The conductivity profile shows excellent agreement with the behavior described on the change of pH. Fig. 2 depicts the faster and higher increase on conductivity when using CO₂ NBs. These results suggest a faster mass transport rate induced by the higher interfacial surface of NBs and their longer contact time.

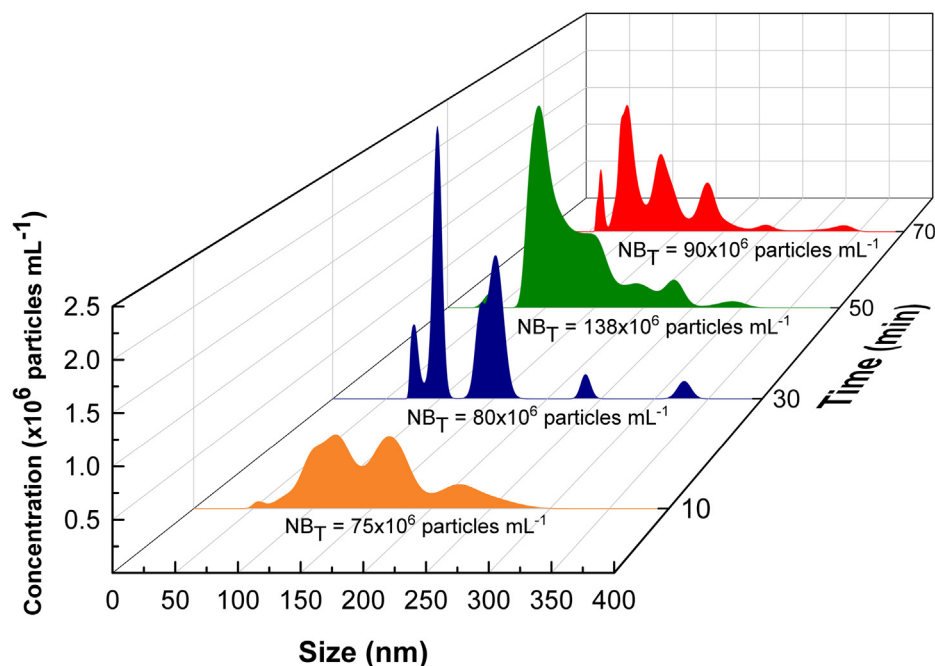
Table 1 presents the pH and conductivity values of samples in stationary mode without turbulence from the pump and measured in a reduced volume of 500 mL of sample. The values were similar to those collected during experimental process, the difference between pH values at 50 and 70 min was 0.03 suggesting the saturation of the system with CO₂ dissolved was attained.

3.2. Evaluating nanobubble size distribution

Nanobubble size distribution is a relevant parameter to understand the bubble physical characteristics of the system. Fig. 3 collects the NB size distribution measured by NTA for samples collected at different times of generation of 10 min, 30 min, 50 min and 70 min. It can be observed a different size distribution depending on the generation time, as commonly reported by other studies [1,32]. The analysis of a blank solution prior NBs generation

Table 1pH and conductivity of samples after different times of bulk nanobubbles generation and direct bubbling of CO₂ macrobubbles.

		0 min	10 min	30 min	50 min	70 min
CO ₂ Nanobubbles	pH	5.82	4.43	4.32	4.26	4.23
	Conductivity ($\mu\text{S cm}^{-1}$)	1.578	18.15	29.56	31.03	31.83
CO ₂ Macrobubbles	pH	5.82	4.81	4.65	4.55	4.50
	Conductivity ($\mu\text{S cm}^{-1}$)	1.578	9.876	13.11	15.28	17.50

**Fig. 3.** Size distribution profile and concentration of CO₂ bulk nanobubbles measured with Nanoparticle track analysis (NTA) at different nanobubble generation times.

shows 14×10^6 particles per mL, but with 0.8 particle per frame suggesting high noise signals. For 10-min sample the size distribution was distributed in two main peaks around 120 and 175 nm, with a smaller quantity of larger NBs of 225 nm. The quantity of smaller NBs increases at 30 min, where the larger number of NBs correspond to those of 75 nm of diameter. However, it can be also observed a slight increase of NBs of ~ 150 nm that may be the result of the coalescence of smaller 75 nm NBs. This hypothesis is supported by the larger polydispersion observed at 50 min and 70 min of generation. It can be inferred that the NBs size depends on the surrounding conditions of pH and carbonate system condition. Note that low concentrations of CO₂/carbonate in solution induces gas-transfer process from nanobubble to solution that can decrease the diameter of the NBs in suspension. Meanwhile, the increasing number of NBs may induce their growth by coalescence and their stability are supported by thermodynamics of bulk nanobubbles [33].

A further analysis of the concentration of NBs in solution defined as number of gas particles per mL corroborates the hypothesis of Ostwald ripening [34] because small ones sacrifice themselves to become larger. Fig. 3 shows that the overall concentration of CO₂ NBs independent of their size increases with time of generation until 50 min. The number of NBs increases from 75×10^6 gas particles mL⁻¹ at 10 min up to 138×10^6 gas particles mL⁻¹ at 50 min. Then, it decreases down to 90×10^6 particles mL⁻¹ at 70 min but of larger diameters.

The evaluation of CO₂ NBs zeta-potential indicates that generated bubbles under acidic conditions of the buffered carbonate system have a negative charge. This result agrees with other gas nanointerfaces reported in literature with negative zeta-

potentials [29,35]. The change in zeta potential for nanobubbles typically follows a sigmoidal behavior where the charges are close to zero around the isoelectric point (IEP) of the bubbles. In this study, the zeta-potential of the solution became slightly more negative for longer times of generation as seen in Fig. 4a, in decreasing order from 2.68 mV at 10 min, -1.45 mV at 30 min, -1.98 mV at 50 min, down to -3.05 mV at 70 min of continuous generation, respectively. The decreasing values of zeta-potential from pH 4.43 to 4.23 can be explained by the more acidic pH that contributes to the increase of negative charge at the interfacial gas surface as well as ascribed to the higher number of nanobubbles in solution. The pH value of each sample plays an important role in zeta-potential values. In this case, each sample have a different pH value according to Table 1 and the signal change from 2.68 mV to -1.45 mV suggests that between these two pH values was the isoelectric point of CO₂ NBs. Measurements of the zeta potential at the different pH in absence of NBs did not show any noticeable variation. These low values of zeta potential suggest the short time stability of CO₂ nanobubbles as reported in literature [6,9]. The observed coalescence of NBs at the tested conditions affirms the little/no electrostatic bubble–bubble repulsion. Due to the buffering capacity of CO₂, the nanobubbles are experiencing coalescence at the pH values where the solutions are fully saturated.

The NBs stability was evaluated by NTA along 6 days as depicted in Fig. 4b. In comparison with other gas NBs such as nitrogen, oxygen and air that have reported stability lives of up to months, the stability of CO₂ NBs was shorter lasting only for few days. The low stability of CO₂ NBs could be explained due to chemical reaction between the nanobubble and water. Thus, potential

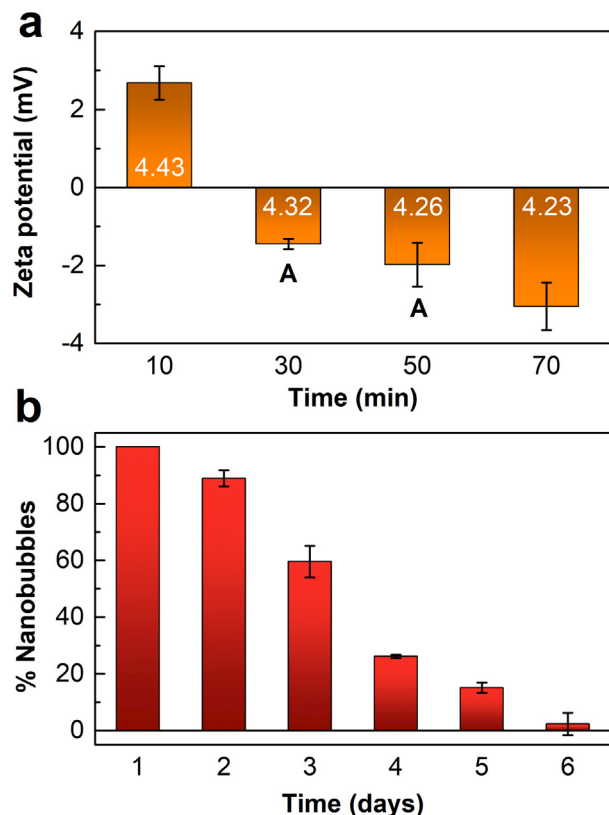


Fig. 4. (a) Zeta potential (mV) measured for CO₂ NBs solution for water samples submitted to different times of continuous NB generation, where the white numbers indicate the experimental pH. (b) Percentage of CO₂ NBs remaining in solution at different days of storage after 50 min of generation (initial content of NBs of 138×10^6 particles mL⁻¹).

application for CO₂ nanobubbles may have to consider continuous generation to maintain the concentration. Stability results have similar values to previously reported ones in the literature [6,10,36]. More than 60% of nanobubbles were lost after 3 days of generation and practically all nanobubbles disappeared after 5 days in our system.

3.3. Unraveling the impact of CO₂ nanobubbles on the buffer capacity

Buffer capacity shows the resistivity of a solution to change the pH by an external agent. In the case of bicarbonate system, the buffer capacity depends on the amount of HCO₃⁻ present in solution. The evaluation of buffer capacity of the bicarbonate system using CO₂ bulk nanobubbles and typical macrobubbles were evaluated via titration of the system as shown in Fig. 5. It can be observed that the blank solution changes its pH by the addition of a base given the lack of buffering capacity of deionized water. As discussed above, the bubbling of CO₂ results in its dissolution and reaction in water according to reactions (1)–(4), which are responsible of the formation of a natural buffer of pH 6 as characteristic of the bicarbonate system given the pK_{a1} of 6.3. The titration curves of Fig. 5a show a widening of the buffering region before reaching the equivalence point with the increased amount of CO₂ delivered to the solution (i.e., longer bubbling times). When comparing the titration curves of solutions bubbled with CO₂ macrobubbles with those exposed to NBs generation (see Fig. 5b) it can be observed a larger difference of the buffering region width for the same time of exposure (cf. Fig. 5c). Considering that the volume of CO₂ gas provided to the system was equal for both procedures (i.e., macrobubbling and nanobubbling) it is obvious that there is a more

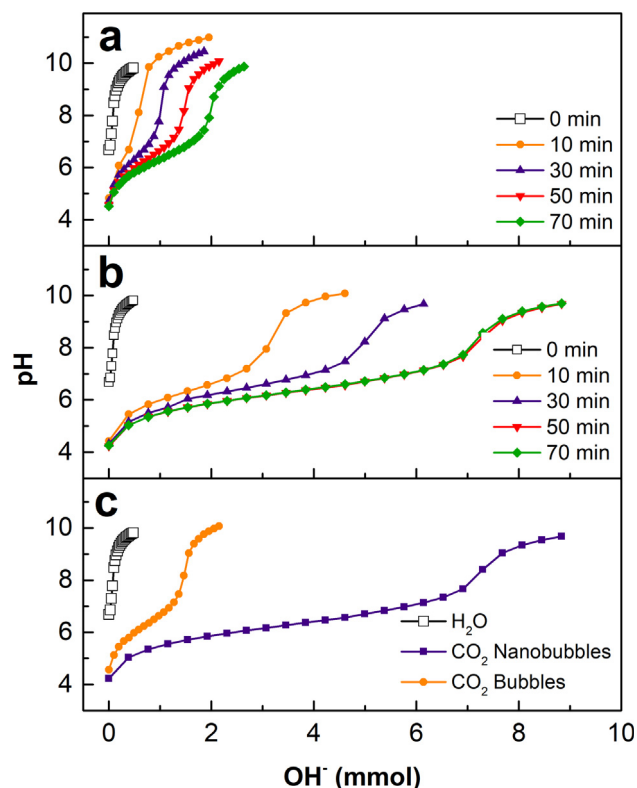


Fig. 5. Titration curves of bicarbonate system generated by (a) CO₂ traditional bubbling and (b) CO₂ bulk nanobubbles. (c) Comparison between nanobubbles and traditional bubbles at 50 min of generation.

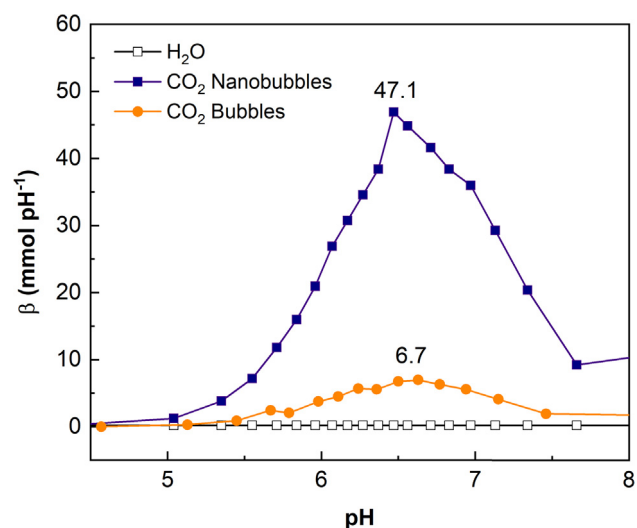


Fig. 6. Buffer capacity evaluation at different pH values of deionized water, CO₂ nanobubbles and CO₂ bubbles.

efficient usage of delivered CO₂ by the NB-system. Note that for samples collected at 50 and 70 min the titration curve displayed practically identical shape pointing to the NB saturation level, which will agree with the larger diameter of NBs at 70 min and decreased number of gas particulates given their coalescence. This result supports the hypothesis that the system may be reaching a pseudo-saturation condition at 50 min of nanobubbles generation. The evaluation of the change of pH over time demonstrated that the NBs are superior in terms of gas transfer to the liquid solution

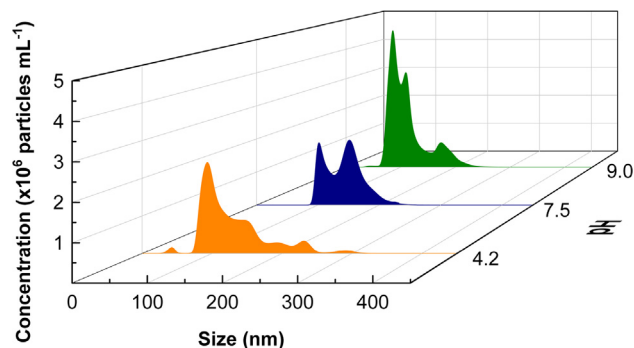


Fig. 7. Nanoparticle track analysis (NTA) showing size distribution and concentration of CO_2 bulk nanobubbles collected after 50 min of generation for the solution adjusted at different pH values of 4.2, 7.5, and 9.0.

(K_1a Nanobubbles $\gg K_1a$ macrobubbles). The NTA measurements also show that NBs have a higher residence time given their unique high stability properties associated to the lack of buoyancy, whereas conventional macrobubbles leave the solution. Then, explaining the higher buffering capacity attained with the NB system.

Fig. 6 shows the buffering capacity (β) of the macrobubble and NBs solutions of CO_2 . The peak of the curve at ~ 6.5 agrees with the characteristic pK_{a1} of the bicarbonate system. However, it can be observed that for a given bubbling time of 50 min there is a huge

difference of β between macro and NBs. This difference suggests that the remaining NBs in solution may be contributing to the buffering capacity of the system to sustain the pH when exposed to an exogenous base (i.e., NaOH). To identify if CO_2 NBs behaves as source of CO_2 during the titration, NTA was carried out at different pH values. Fig. 7 presents the size distribution and concentration of NBs when the solution generated after 50 min at natural pH of 4.2 is adjusted at 7.5, and 9.0. The number of NBs decreases when increasing the solution pH at 7.5 while the polydispersed size distribution becomes more uniform showing two major size distributions around NBs diameter of 100 nm and 150 nm. This result suggests that the change in pH causes the NBs to decrease their number because of the gas dissolution induced by the equilibria displacement of reactions (1)–(4) upon the addition of NaOH . Further increase in pH up to 9.0 shows an unexpected increase of number of NBs but of smaller size mainly within the range of 70 nm and 100 nm. Fig. 8 shows NTA frames observed at different pH values that demonstrate different size and number of particles per frame. In agreement with the values reported in Fig. 7, it can be observed that the frames at pH 9.0 show higher number of NBs of smaller size. This can be *a priori* a contradictory finding, but the calculation of the total volume of gas depicted in Fig. 9 evidence the consumption of CO_2 gas. Note that a higher concentration of gas NBs of smaller diameter do not represent a higher volume of gas contained in solution, thus these results hint to the role of NBs as additional chemical source that contribute to enlarge the buffer capacity of the system when compared to conventional buffered systems through CO_2 bubbling. The measurements of the

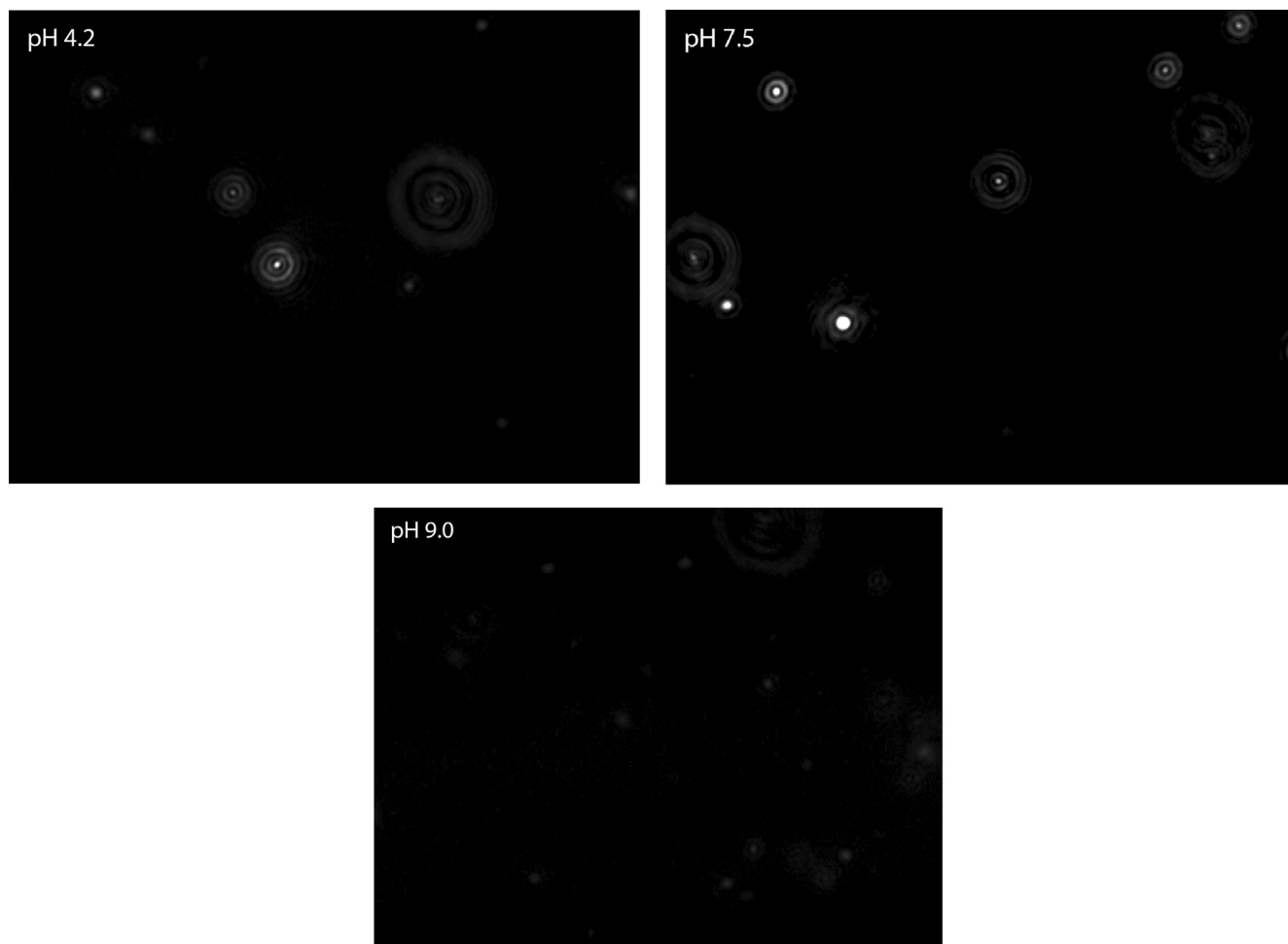


Fig. 8. NTA images of CO_2 bulk nanobubbles collected after 50 min of generation for the solution adjusted at different pH values of 4.2, 7.5, and 9.0.

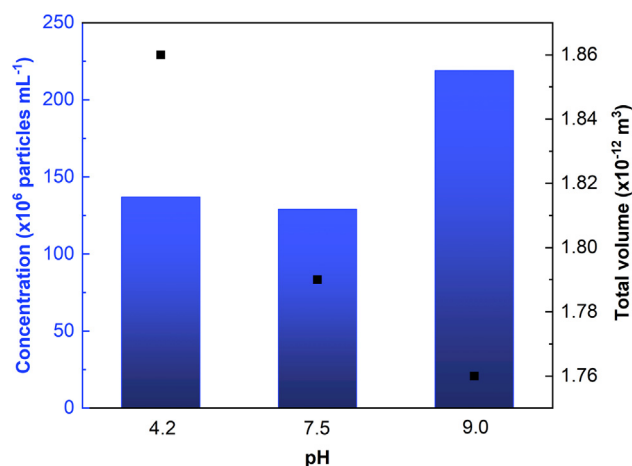


Fig. 9. Concentration of NBs measured in solution as gas particles per unit volume of a solution where NBs are generated for 50 min and then pH is adjusted by the addition of NaOH from initial pH 4.2 up to 7.5 and 9.0. The graph also depicts the total volume of gas contained in the solution that decreases with increasing pH.

NTA suggest an increase on nanobubble amount at alkaline pH given the shrinking of the gas pockets, but at the same time results in less volume of $\text{CO}_{2(g)}$ suspended within NBs in the solution. It may be hypothesized that the change of pH may contribute to the NBs scission and shrinking. Shrinking may be induced by the forced transport of $\text{CO}_{2(g)}$ contained in the NBs towards solution to resist alkalization in response to the addition of base. However, more research should be conducted on that regard to further confirm this initial hypothesis. The size decrease of CO_2 NBs at higher pH supports the hypothesis that gas-transfer still occurs from bubble to solution until as deduced from the reduction of average NB diameter, which may occur till their total disappearance.

4. Conclusions

In this study, CO_2 nanobubbles mass transfer and reactivity were evaluated at different generation times (10, 30, 50, and 70 min). Previous reports evaluated the stability, interaction with different electrolytes, size distribution, zeta potential, and viscosity [4,6,9,12,26,36]. However, the gas-transfer process and chemical reaction were not evaluated for CO_2 NBs, this is the first-time reporting both values. Gas-transfer depends on specific surface area of bubbles in water. Thus, CO_2 nanobubbles have a fast gas-transfer from nanobubble to solution until system saturation. This was evaluated using the mass transfer coefficient ($K_L a$) that for the same inlet amount of gas to the system $K_L a$ for nanobubbles is 11-fold comparatively to traditional bubbles. However, nanobubbles remaining in the solution dependant on time generation and pH. Size distribution present different sizes of nanobubbles in a range of 75 to 250 nm. This value range could be considered result of Oswaldt ripening to increase the nanobubble size or gas-transfer process to reduce it.

An important outcome of this study is that the effective amount of CO_2 in the form of HCO_3^- present in solution was quantified as buffer capacity. Nanobubbles present a 7-fold buffer capacity than traditional bubbles due to nanobubbles works as CO_2 source. The NBs behavior during chemical reaction was studied by NTA. According to the results, nanobubbles work as CO_2 source reducing their size and changing the electrical surrounding at different pH values. These results are expected to be useful for applications in CO_2 starving systems [20], buffer solutions [6], and water treatment [8]. Further studies are required to evaluate the effect of dif-

ferent water matrix in the gas-transfer and buffer capacity of CO_2 NBs.

CRediT authorship contribution statement

Gabriel Antonio Cerrón-Calle: Conceptualization, Methodology, Validation, Investigation, Formal analysis, Data curation, Visualization, Writing – original draft. **Andre Luna Magdaleno:** Conceptualization, Methodology, Investigation, Formal analysis, Data curation, Writing – original draft. **John C. Graf:** Conceptualization, Methodology, Validation, Writing – review & editing. **Onur G. Apul:** Conceptualization, Methodology, Validation, Visualization, Writing – review & editing, Supervision, Project administration, Funding acquisition. **Sergi Garcia-Segura:** Conceptualization, Methodology, Data curation, Resources, Visualization, Writing – original draft, Writing – review & editing, Supervision, Project administration, Funding acquisition.

Declaration of Competing Interest

The authors declare that they have no known competing financial interests or personal relationships that could have appeared to influence the work reported in this paper.

Acknowledgments

The authors thank the financial support provided by NASA through the Maine Space Grant Consortium (MSGC) project EP-22-01. Any opinions, findings, and conclusions or recommendations expressed in this material are those of the authors and do not necessarily reflect the views of the National Aeronautics and Space Administration or of the Maine Space Grant Consortium. A.L. Magdaleno and S. Garcia-Segura thank the support of the Western Alliance to Expand Student Opportunities (WAESO) Louis Stokes Alliance for Minority Participation (LSAMP) National Science Foundation (NSF) Cooperative Agreement No. HRD-1619524. Authors would like to acknowledge Yanyang Tang and Ian Shoemaker for the valuable training and experience on the use of the nanotrack analyzer (NTA). Authors are thankful for the discussions with Dr. Christopher M. Matty and Dr. Emily Matula.

References

- [1] E.P. Favvas, G.Z. Kyzas, E.K. Efthimiadou, A.C. Mitropoulos, Bulk nanobubbles, generation methods and potential applications, *Curr. Opin. Colloid Interface Sci.* 54 (2021), <https://doi.org/10.1016/j.cocis.2021.101455> 101455.
- [2] D.V.B. Batchelor, F.J. Armistead, N. Ingram, S.A. Peyman, J.R. McLaughlan, P.L. Coletta, et al., Nanobubbles for therapeutic delivery: Production, stability and current prospects, *Curr. Opin. Colloid Interface Sci.* 54 (2021), <https://doi.org/10.1016/j.cocis.2021.101456> 101456.
- [3] B.H. Tan, H. An, C.D. Ohl, Stability of surface and bulk nanobubbles, *Curr. Opin. Colloid Interface Sci.* 53 (2021), <https://doi.org/10.1016/j.cocis.2021.101428> 101428.
- [4] S.H. Oh, J.M. Kim, Generation and Stability of Bulk Nanobubbles, *Langmuir* 33 (2017) 3818–3823, <https://doi.org/10.1021/acs.langmuir.7b00510>.
- [5] E.D. Michailidi, G. Bomis, A. Varoutoglou, G.Z. Kyzas, G. Mitrikas, A.C. Mitropoulos, et al., Bulk nanobubbles: Production and investigation of their formation/stability mechanism, *J. Colloid Interface Sci.* 564 (2020) 371–380, <https://doi.org/10.1016/j.jcis.2019.12.093>.
- [6] K.K.T. Phan, T. Truong, Y. Wang, B. Bhandari, Formation and Stability of Carbon Dioxide Nanobubbles for Potential Applications in Food Processing, *Food Eng. Rev.* 13 (2021) 3–14, <https://doi.org/10.1007/s12393-020-09233-0>.
- [7] F.Y. Ushikubo, T. Furukawa, R. Nakagawa, M. Enari, Y. Makino, Y. Kawagoe, et al., Evidence of the existence and the stability of nano-bubbles in water, *Colloids Surfaces Physicochem. Eng. Asp* 361 (2010) 31–37, <https://doi.org/10.1016/j.colsurfa.2010.03.005>.
- [8] A.J. Atkinson, O.G. Apul, O. Schneider, S. Garcia-Segura, P. Westerhoff, Nanobubble Technologies Offer Opportunities to Improve Water Treatment, *Acc. Chem. Res.* (2019), <https://doi.org/10.1021/acs.accounts.8b00606>.
- [9] Y. Zhou, Z. Han, C. He, Q. Feng, K. Wang, Y. Wang, et al., Long-term stability of different kinds of gas nanobubbles in deionized and salt water, *Materials (Basel)* 14 (2021), <https://doi.org/10.3390/ma14071808>.

- [10] Q. Wang, H. Zhao, N. Qi, Y. Qin, X. Zhang, Y. Li, Generation and Stability of Size-Adjustable Bulk Nanobubbles Based on Periodic Pressure Change, *Sci. Rep.* 9 (2019) 1–9, <https://doi.org/10.1038/s41598-018-38066-5>.
- [11] X. Ji, C. Liu, G. Pan, Interfacial oxygen nanobubbles reduce methylmercury production ability of sediments in eutrophic waters, *Ecotoxicol. Environ. Saf.* 188 (2020), <https://doi.org/10.1016/j.ecoenv.2019.109888>.
- [12] T. Fujita, H. Kurokawa, Z. Han, Y. Zhou, H. Matsui, J. Ponou, et al., Free radical degradation in aqueous solution by blowing hydrogen and carbon dioxide nanobubbles, *Sci. Rep.* 11 (2021) 1–13, <https://doi.org/10.1038/s41598-021-82717-z>.
- [13] P. Sobieszuk, A. Strzyżewska, K. Ulatowski, Investigation of the possibility of culturing aerobic yeast with oxygen nanobubble addition and evaluation of the results of batch and semi-batch cultures of *Saccharomyces cerevisiae*, *Chem. Eng. Process. Process. Intensif.* 159 (2021), <https://doi.org/10.1016/j.cep.2020.108247>.
- [14] H. He, L. Zheng, Y. Li, W. Song, Research on the Feasibility of Spraying Micro/Nano Bubble Ozonated Water for Airborne Disease Prevention, *Ozone Sci. Eng.* 37 (2015) 78–84, <https://doi.org/10.1080/01919512.2014.913473>.
- [15] J. Al-Gousous, K.X. Sun, D.P. McNamara, B. Hens, N. Salehi, P. Langguth, et al., Mass Transport Analysis of the Enhanced Buffer Capacity of the Bicarbonate-CO₂ Buffer in a Phase-Heterogenous System: Physiological and Pharmaceutical Significance, *Mol. Pharm.* 15 (2018) 5291–5301, <https://doi.org/10.1021/acs.molpharmaceut.8b00783>.
- [16] J. Wu, K. Zhang, C. Cen, X. Wu, R. Mao, Y. Zheng, Role of bulk nanobubbles in removing organic pollutants in wastewater treatment, *AMB Express.* 11 (2021), <https://doi.org/10.1186/s13568-021-01254-0>.
- [17] A. Singh, A.S. Sekhon, P. Unger, M. Babb, Y. Yang, M. Michael, Impact of gas micro-nano-bubbles on the efficacy of commonly used antimicrobials in the food industry, *J. Appl. Microbiol.* 130 (2021) 1092–1105, <https://doi.org/10.1111/jam.14840>.
- [18] W. Fan, Y. Li, C. Wang, Y. Duan, Y. Huo, B. Januszewski, et al., Enhanced Photocatalytic Water Decontamination by Micro-Nano Bubbles: Measurements and Mechanisms, *Environ. Sci. Technol.* (2021), <https://doi.org/10.1021/acs.est.0c08787>.
- [19] T. Hou, J. Zhao, Z. Lei, K. Shimizu, Z. Zhang, Addition of air-nanobubble water to mitigate the inhibition of high salinity on co-production of hydrogen and methane from two-stage anaerobic digestion of food waste, *J. Clean Prod.* 314 (2021), <https://doi.org/10.1016/j.jclepro.2021.127942>.
- [20] T. Tang, P. Wan, Z. Hu, CO₂ Bubbling to Improve Algal Growth, Nutrient Removal, and Membrane Performance in an Algal Membrane Bioreactor, *Water Environ. Res.* 90 (2018) 650–658, <https://doi.org/10.2175/106143017x15131012153121>.
- [21] M. Kordač, V. Linek, Dynamic measurement of carbon dioxide volumetric mass transfer coefficient in a well-mixed reactor using a pH probe: Analysis of the salt and supersaturation effects, *Ind. Eng. Chem. Res.* 47 (2008) 1310–1317, <https://doi.org/10.1021/ie0711776>.
- [22] G.A. Hill, Measurement of overall volumetric mass transfer coefficients for carbon dioxide in a well-mixed reactor using a pH probe, *Ind. Eng. Chem. Res.* 45 (2006) 5796–5800, <https://doi.org/10.1021/ie060242t>.
- [23] D. Wolff-Boenisch, On the buffer capacity of CO₂-charged seawater used for carbonation and subsequent mineral sequestration, *Energy Procedia.* 4 (2011) 3738–3745, <https://doi.org/10.1016/j.egypro.2011.02.307>.
- [24] L.Q. Jiang, B.R. Carter, R.A. Feely, S.K. Lauvset, A. Olsen, Surface ocean pH and buffer capacity: past, present and future, *Sci. Rep.* 9 (2019) 1–11, <https://doi.org/10.1038/s41598-019-55039-4>.
- [25] E.D. Revellame, R. Aguda, A. Chistoserdov, D.L. Fortela, R.A. Hernandez, M.E. Zappi, Microalgae cultivation for space exploration: Assessing the potential for a new generation of waste to human life-support system for long duration space travel and planetary human habitation, *Algal. Res.* 55 (2021) 6–11, <https://doi.org/10.1016/j.algal.2021.102258>.
- [26] K. Phan, T. Truong, Y. Wang, B. Bhandari, Effect of CO₂ nanobubbles incorporation on the viscosity reduction of fruit juice concentrate and vegetable oil, *Int. J. Food Sci. Technol.* (2021) 1–9, <https://doi.org/10.1111/ijfs.15240>.
- [27] Yamaguchi M, Ma T, Tadaki D, Hirano-iwata A, Watanabe Y, Kanetaka H, et al. Bactericidal Activity of Bulk Nanobubbles through Active Oxygen Species Generation 2021. <https://doi.org/10.1021/acs.langmuir.1c01578>
- [28] M. Takahashi, Y. Shirai, S. Sugawa, Free-Radical Generation from Bulk Nanobubbles in Aqueous Electrolyte Solutions: ESR Spin-Trap Observation of Microbubble-Treated, Water (2021), <https://doi.org/10.1021/acs.langmuir.1c00469>.
- [29] A.K.A. Ahmed, C. Sun, L. Hua, Z. Zhang, Y. Zhang, T. Marhaba, et al., Colloidal Properties of Air, Oxygen, and Nitrogen Nanobubbles in Water: Effects of Ionic Strength, Natural Organic Matters, and Surfactants, *Environ. Eng. Sci.* 35 (2018) 720–727, <https://doi.org/10.1089/ees.2017.0377>.
- [30] F.Y. Ushikubo, M. Enari, T. Furukawa, R. Nakagawa, Y. Makino, Y. Kawagoe, et al., Zeta-potential of micro- and/or nano-bubbles in water produced by some kinds of gases, *IFAC Proc.* 3 (2010), <https://doi.org/10.3182/20101206-3-jp-3009.00050>.
- [31] L. Parkinson, R. Sedev, D. Fornasiero, J. Ralston, The terminal rise velocity of 10–100 µm diameter bubbles in water, *J. Colloid Interface Sci.* 322 (2008) 168–172, <https://doi.org/10.1016/j.jcis.2008.02.072>.
- [32] M. Li, X. Ma, J. Eisener, P. Pfeiffer, C.D. Ohl, C. Sun, How bulk nanobubbles are stable over a wide range of temperatures, *J. Colloid Interface Sci.* 596 (2021) 184–198, <https://doi.org/10.1016/j.jcis.2021.03.064>.
- [33] T. Vehmas, L. Makkonen, Metastable Nanobubbles (2021), <https://doi.org/10.1021/acsomega.0c05384>.
- [34] S. Tcholakova, F. Mustan, N. Pagureva, K. Golemanov, N.D. Denkov, E.G. Pelan, et al., Role of surface properties for the kinetics of bubble Ostwald ripening in saponin-stabilized foams, *Colloids Surfaces A Physicochem Eng Asp* 534 (2017) 16–25, <https://doi.org/10.1016/j.colsurfa.2017.04.055>.
- [35] M. Takahashi, ζ Potential of microbubbles in aqueous solutions: Electrical properties of the gas - Water interface, *J. Phys. Chem. B* 109 (2005) 21858–21864, <https://doi.org/10.1021/jp0445270>.
- [36] K. Phan, T. Truong, Y. Wang, B. Bhandari, Effect of electrolytes and surfactants on generation and longevity of carbon dioxide nanobubbles, *Food Chem.* 130299 (2021), <https://doi.org/10.1016/j.foodchem.2021.130299>.